Batteries & Supercaps

Research Article
doi.org/10.1002/batt.202500495

Chemistry Europe
European Chemical Societies Publishing

www.batteries-supercaps.org

Interface Engineering via $Li_2C_4O_4$ Prelithiation: Boosting Activated Carbon Electrode Performance in Lithium-Ion Capacitors

Miguel Granados-Moreno, Rosalía Cid,* Julia Maibach, Maria Arnaiz, Eider Goikolea, and Jon Ajuria*

Pre-lithiation is an essential step in lithium-ion capacitors (LICs) due to the lack of Li^+ in both electrodes. The integration of dilithium squarate ($Li_2C_4O_4$) into the positive electrode of LICs is considered one of the most promising pre-lithiation strategies. Therefore, the ability of $Li_2C_4O_4$ decomposition products to modify the solid electrolyte interphase has been recently disclosed, although their impact on the positive electrode surface has not been studied yet. In this work, the improvement of the electrochemical performance when $Li_2C_4O_4$ was included has been investigated by analyzing the surface of activated carbon-based electrodes with and without $Li_2C_4O_4$ by scanning electron microscopy and X-ray photoelectron spectroscopy. The decomposition of $Li_2C_4O_4$ leads to the formation of a surface layer on the positive electrode that remains unaltered regardless of the applied potential, as well as after an aging test. Thus, the improved electrochemical performance is attributed to the presence of a pseudocapacitive charge storage mechanism enabled by the surface layer. Lastly, the cells are modified to reveal the main components participating in the surface layer formation. These findings provide valuable insights into the impact, benefits, and limitations of $Li_2C_4O_4$, which will accelerate the development of other suitable alternative sacrificial salts.

1. Introduction

Lithium-ion capacitors (LICs) are hybrid devices that combine lithium-ion batteries (LIBs) and electrical double-layer capacitors (EDLCs), being able to deliver high energy density while operating at high power density. Since their invention in 2001,[1] the interest in LIC technology has grown considerably both in terms of academic publications and commercial devices.[2] The latter remains a challenge owing to the architecture of LICs. The absence of lithium in both the negative and positive electrodes of LICs leads to the depletion of Li^+ in the electrolyte during the cell operation. Thus, a pre-lithiation step prior to cell operation is essential to incorporate the Li^+ required to compensate for the first cycle irreversibility and solid electrolyte interphase (SEI) formation in the negative electrode.[3–5] This step is also necessary to adjust the negative electrode potential to enlarge the cell voltage and, consequently, increase the energy density.

Over the past years, several pre-lithiation strategies have been developed aiming to improve performance, scalability, and cost of LICs.[6] Among these strategies, dilithium squarate ($Li_2C_4O_4$) was reported by Arnaiz et al. as an easily synthesized, cost-effective, safe, and air-stable additive for LICs pre-lithiation.[4] $Li_2C_4O_4$ can be processed in air together with the other components of the positive electrode, and it does not present chemical incompatibilities with common solvents used for electrode fabrication nor with electrolytes. $Li_2C_4O_4$ has been mostly integrated in activated carbon (AC) electrodes, although it has also been used in hybrid electrodes.[7,8] $Li_2C_4O_4$ has been demonstrated to be a versatile and transversal pre-lithiation method, suitable for use with various chemistries and processing methods. In this regard, $Li_2C_4O_4$ decomposes as a sacrificial salt in the range of 3.9—4.2 V *vs* Li^+/Li, releasing Li^+, gaseous CO_2 and CO, and carbon deposits.[9,10] In previous studies, CO_2 has been used as a film-forming additive in the form of dry ice or by assembling the cells in a CO_2-rich atmosphere, as reported for LIBs.[11–14] Recently, the influence of $Li_2C_4O_4$ pre-lithiation additive in the chemical composition of the SEI was disclosed.[15] Thus, decomposition by-products of $Li_2C_4O_4$ are dissolved in the electrolyte and modify the SEI composition. The modified SEI was functional and stable under different conditions, with a high amount of oxygenated compounds. Similar compounds might be formed on the positive electrode when $Li_2C_4O_4$ is used. Furthermore, an electrochemical performance enhancement has been reported in AC-$Li_2C_4O_4$ electrodes with respect to bare AC electrodes, with better rate

M. Granados-Moreno, R. Cid, M. Arnaiz, J. Ajuria
Centre for Cooperative Research on Alternative Energies (CIC energiGUNE)
Basque Research and Technology Alliance (BRTA)
Alava Technology Park, Albert Einstein 48, 01510 Vitoria-Gasteiz, Spain
E-mail: rcid@cicenergigune.com
jajuria@cicenergigune.com

M. Granados-Moreno, E. Goikolea
Department of Organic and Inorganic Chemistry
Faculty of Science and Technology
University of the Basque Country UPV/EHU
48940 Leioa, Spain

J. Maibach
Department of Physics
Chalmers University of Technology
41296 Gothenburg, Sweden

Supporting information for this article is available on the WWW under https://doi.org/10.1002/batt.202500495

capability and ca. 20% capacity increase.[6] The exact causes of this enhancement are unknown, but some hypotheses include the modification of the electrode microstructure by the voids left after $Li_2C_4O_4$ decomposition[6]; or the functionalization of the AC surface by the influence of $Li_2C_4O_4$.

Given the SEI modification observed in the negative electrode, the decomposition of $Li_2C_4O_4$ could also impact the properties of the positive electrode surface. In this regard, the interaction of released CO_2 and CO with the electrolyte at the positive electrode surface may lead to the formation of functional groups and, broadly, modify the surface chemistry of the electrode. This functionalization of the surface might contribute to charge storage through pseudocapacitive mechanisms, potentially explaining the observed increases in capacity and rate capability performance. Pseudocapacitive charge storage mechanisms can be divided into two groups depending on where the reaction occurs: Intercalation pseudocapacitance and surface pseudocapacitance. In intercalation pseudocapacitance, fast faradaic reactions take place in the bulk of the electrode, usually in layered materials such as Nb_2O_5 or Ti_3C_2, where the crystalline structure allows fast insertion and deinsertion of Li^+.[16] In surface pseudocapacitance, the surface of redox-active materials (AMs), as RuO_2 or MnO_2,[17,18] is reduced/oxidized upon cycling. AC functionalization has been extensively studied to improve the electrode properties of EDLCs and LICs. For example, functionalization of the AC surface with phosphate or phosphonate groups results in improved charge transport capability and enhanced charge storage due to an added pseudocapacitive component.[19] Doping and co-doping AC with heteroatoms like phosphorus, oxygen, nitrogen, or sulfur are also well-known strategies to improve the AC electrical properties.[20–22] Oxygen-doping of AC has also been reported to improve the electrochemical performance of the electrodes, mainly due to the enhanced pseudocapacitance provided by the action of C═O, C—OH, and COOH functional groups in aqueous electrolyte.[23–26] In fact, the quinone-hydroquinone system is the best-known example of pseudocapacitive mechanism in AC electrodes, where quinone is reduced into hydroquinone by its reaction with two H^+ and two e^-. Nevertheless, oxygen amounts must be carefully controlled in order to maintain high conductivity and long cycle life. Unfortunately, most of the pseudocapacitive mechanisms presented above require, and are therefore dependent on, aqueous electrolytes.[27] While surface pseudocapacitance can also occur in organic electrolytes,[26,28,29] its contribution to the total capacity is usually low, and the underlying charge storage mechanisms are not yet fully understood.[30]

The high contact area between the AC electrode and the electrolyte is crucial, as it is where the charge storage of supercapacitors occurs.[31,32] Furthermore, the interface between electrode and electrolyte is a major site for decomposition reactions, due to the interaction of electrode and electrolyte molecules and the electrical potential gradient.[33–35] Thus, it is of utmost importance to understand the implications of using $Li_2C_4O_4$ and the role of its decomposition products at the interfaces. To the best of our knowledge, the influence of $Li_2C_4O_4$ sacrificial salt decomposition products on the AC electrode surface has never been studied. In this work, X-ray Photoelectron Spectroscopy (XPS) has been employed to study the chemical composition of the electrode surface, unveiling the possible formation of an electrode–electrolyte interphase. XPS is a very sensitive technique for detecting superficial chemical changes and has been widely used in characterizing both negative and positive electrode surfaces.[36] For LIC positive electrodes, it has been used to analyze the chemical composition of doped and functionalized AC.[37,38]

Therefore, XPS has also been used to perform antemortem and postmortem studies, which are particularly interesting since the formation of a surface layer on top of the AC electrode is commonly considered one of the main degradation mechanisms in LICs and EDLCs.[33,34] In this regard, Ishimoto et al.[39] studied the degradation mechanisms of EDLCs using 1 M triethylmethylammonium tetrafluoroborate (TEMA BF_4) in propylene carbonate (PC) based electrolyte. The degradation mechanisms occurring at the positive electrode result in PC electrolysis, releasing CO_2 and CO, and forming a resistive layer on top of the electrode surface. In addition, H_2 and OH^- were formed from PC reduction at the negative electrode surface, accelerating PC decomposition and triggering the formation of other decomposition products. Similar behavior is reported for ethylene carbonate (EC), dimethyl carbonate (DMC), and other carbonate-based electrolytes, where solvent decomposition leads to the formation of a passivation layer on the electrode surface, primarily composed of polycarbonates.[40,41] However, the surface of positive electrodes containing $Li_2C_4O_4$ has been little studied. One of the few reports was carried out by Gomez-Martin et al.[7] based on XPS analysis of pristine NMC-$Li_2C_4O_4$ positive electrodes and cycled electrodes after $Li_2C_4O_4$ decomposition. A decrease in fluorinated species was observed, together with an increase in the amount of C—O and carbonate species at the surface. However, the specific influence of $Li_2C_4O_4$ on the surface composition has not been isolated from the impact of the electrolyte or the rest of the components of the cell, and the implications of the electrode surface modification on the electrochemical performance have not been fully determined.

In this work, the AC-$Li_2C_4O_4$ positive electrode surfaces have been studied to elucidate the origin of the electrochemical performance improvement and determine the impact of $Li_2C_4O_4$ decomposition by-products on the electrode surface modification. For comparison, bare AC electrodes without $Li_2C_4O_4$ have also been characterized, applying similar cycling protocols. XPS analysis of the AC-$Li_2C_4O_4$ electrode surface revealed the formation of a surface layer due to the interaction of $Li_2C_4O_4$ decomposition products with the electrolyte. The surface layer has been extensively characterized under different electrochemical conditions to examine its stability. In addition, the electrode and electrolyte were modified by replacing fluorinated components to enlighten the formation process of the surface layer. The chemistry and evolution of the surface layer composition during charge and discharge allow hypothesizing about the pseudocapacitive mechanism taking place on the electrodes. Thus, the chemical composition of the surface layer formed on the AC-$Li_2C_4O_4$ electrodes has been revealed, elucidating the role of the different electrode and electrolyte components in its formation, and its impact on the electrochemical performance has been analyzed.

Research Article
doi.org/10.1002/batt.202500495
Chemistry Europe
European Chemical Societies Publishing

2. Results

2.1. Electrochemical Performance

The principal reason for incorporating $Li_2C_4O_4$ in the positive electrode is to facilitate the pre-lithiation of LICs.[3,6,42] During the first charge of the cell, $Li_2C_4O_4$ is decomposed at *ca.* 3.9 V *vs.* Li^+/Li, delivering Li^+, releasing gaseous CO_2 and CO, and forming carbon deposits as described in **Equation (1)**.[10] Li^+ migrates to the electrolyte and the negative electrode, contributing to SEI formation and adjusting the negative electrode potential. Meanwhile, CO_2 and CO partially dissolve into the electrolyte, while most of them remain in the gaseous phase and can be removed through a degassing step.

$$Li_2C_4O_4 \rightarrow 1.47CO_2 + 1.06CO + 1.47C + 2Li^+ \quad (1)$$

In addition to providing the extra lithium amount needed for pre-lithiation, the decomposition of $Li_2C_4O_4$ is reported to positively affect the electrochemical performance of AC-based positive electrodes.[6] **Figure 1** shows the electrochemical characterization of AC-$Li_2C_4O_4$ and AC electrodes in a half-cell configuration, aimed at isolating the influence of $Li_2C_4O_4$ on the electrode performance. Prior to the electrochemical characterization of AC-$Li_2C_4O_4$, 10 cycles at $C_{Li2C4O4}/10$ ($C_{Li2C4O4} = 425$ mAh g^{-1}) were performed to decompose the sacrificial salt as depicted in Figure 1a. The decomposition of $Li_2C_4O_4$ can be clearly seen in the first cycle between 3.8 and 4.2 V. $Li_2C_4O_4$ decomposes almost completely in the first cycle, although some additional cycles are required, as signaled by the distorted galvanostatic charge–discharge (GCD) of the next cycles. Figure 1b shows the GCD curves of AC-$Li_2C_4O_4$ and AC between 2 and 4.2 V *vs.* Li^+/Li. Although both samples show a triangular shape, AC-$Li_2C_4O_4$ clearly possesses larger charge and discharge times at any applied current density. Figure 1c depicts the cyclic voltammetry (CV) curves of AC-$Li_2C_4O_4$ and AC electrodes at 5 mV s^{-1}, with the AC-$Li_2C_4O_4$ sample registering larger current density. Both samples show the characteristic quadratic shape CVs; nevertheless, AC-$Li_2C_4O_4$ is characterized by a little deviation around 3.5 V versus Li^+/Li during the charge step, which could be related to the capacity increase illustrated in Figure 1d. Figure 1d depicts the rate capacity of AC-$Li_2C_4O_4$ and AC, which registered a *ca.* 20% capacity increase once the sacrificial salt is decomposed. In addition, capacity retention over the applied current density is improved for AC-$Li_2C_4O_4$, which delivers ca. 72 mAh g^{-1} at 3 A g^{-1}. Different factors might account for the electrochemical performance enhancement: i) A specific surface area (SSA) increase during $Li_2C_4O_4$ decomposition: this option has already been studied by Pan et al.[1], who discarded the idea that the SSA of AC-$Na_2C_4O_4$ could increase with respect to AC fresh electrodes, due to the formation of carbon deposits during the sacrificial salt decomposition. In fact, those carbon deposits contribute to blocking the micropore entrances, decreasing the SSA; ii) Conductivity enhancement due to the decomposition of the $Li_2C_4O_4$. The decomposition of the sacrificial salt creates voids in the structure of the electrode, modifying its textural properties, as reported by Scanning Electron Microscopy (SEM) and nitrogen adsorption/desorption isotherms.[6,10] Thus, the changes in the electrode might reduce the diffusion resistance and improve the overall electrode conductivity.[43,44] Electrochemical impedance spectroscopy (EIS) measurements were performed to elucidate the conductivity of AC and AC-$Li_2C_4O_4$ electrodes. Figure 1e shows the Nyquist plot of AC-$Li_2C_4O_4$ and AC after 10 GCD cycles. AC-$Li_2C_4O_4$ was cycled at $C_{Li2C4O4}/10$ between 2 and 4.2 V *vs* Li^+/Li, to ensure the decomposition of $Li_2C_4O_4$, while for AC, a current

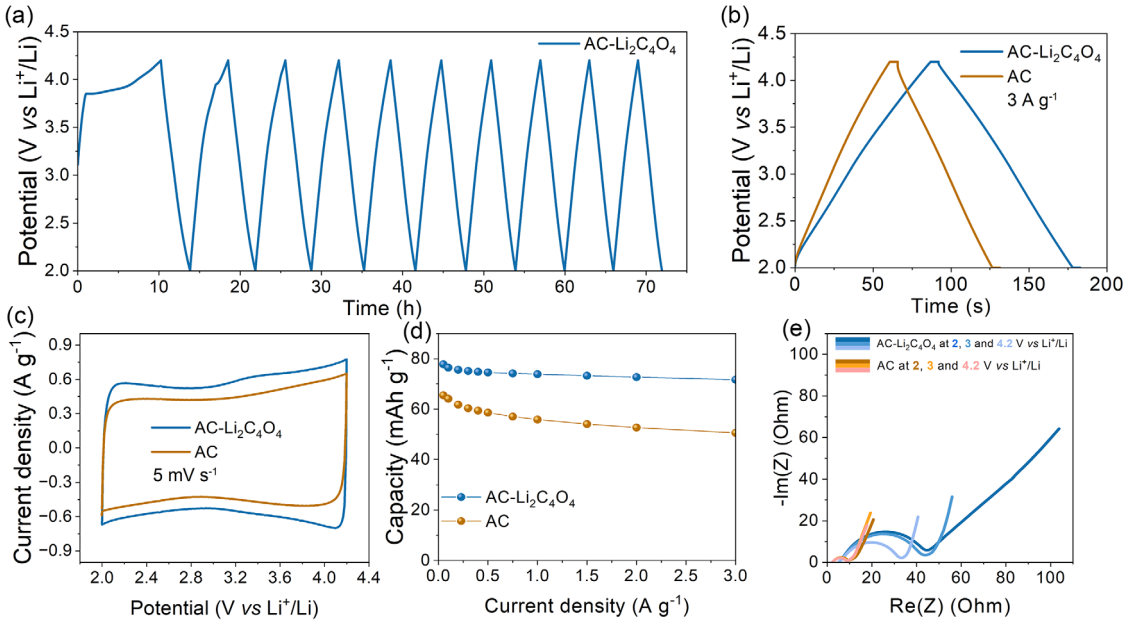

Figure 1. Electrochemical characterization of AC-$Li_2C_4O_4$ (blue) and AC (brown): a) GCD during the $Li_2C_4O_4$ decomposition protocol; b) GCD curves at 3 A g^{-1}; c) CV at 5 mV s^{-1}; d) rate capability between 0.05 and 3 A g^{-1}; and e) PEIS at 2, 3, and 4.2 V vs Li^+/Li.

density of 0.01 A g^{-1} was selected instead. The samples, including $Li_2C_4O_4$, were characterized by higher resistance values in comparison to those of bare AC, regardless of the electrode potential. Thus, an enhancement in electrode conductivity or ion absorption kinetics is unlikely to be the mechanism improving the rate capability of AC-$Li_2C_4O_4$; iii) Another possible explanation is the formation of functional groups on the electrode surface that might induce pseudocapacitive mechanisms.[45] As discussed in the introduction, CO_2 and CO decomposition products formed during $Li_2C_4O_4$ decomposition might react with the electrolyte to form certain functional groups in the electrode surface.

Recently, we revealed the ability of CO_2 and CO, decomposition products of the $Li_2C_4O_4$ sacrificial salt, to modify the negative electrode surface composition.[15] Briefly, CO_2 and CO dissolve into the electrolyte and react with it at the hard carbon (HC) surface, increasing the amount of O═C-O, C═O, and C—O species in the SEI. A similar effect may occur in the positive electrode, resulting in surface functionalization and enhancement of electrochemical performance. The formation of a surface layer might be responsible for the observed increase in resistance, explaining the larger resistance in the AC-$Li_2C_4O_4$ electrode. In addition, the resistance varies with the potential, suggesting that transport properties through the surface layer might be different for each ion (i.e., Li^+ and PF_6^-). The electrochemical differences between samples with and without $Li_2C_4O_4$ described above suggest the presence of a pseudocapacitive mechanism, which may change both the composition and the properties of the electrode surface. A large number of samples were studied to elucidate this phenomenon. Abbreviations are listed in **Table 1** to aid the readability of the following sections.

Table 1. List of abbrebiations.

Abbreviations	Definitions
LIC	Lithium ion capacitor
HC	Hard carbon
AC	AC electrodes containing conducting carbon and PvDF
AC-4.2V	AC electrode charged at 4.2 V
AC-2.5V	AC electrode discharged at 2.5 V
AC_{CMC}	AC electrodes containing conducting carbon and CMC
$Li_2C_4O_4$	Dilithium squarate
AC- $Li_2C_4O_4$	AC + conducting carbon + PvDF electrode incorporating dilithium squarate
AC_{CMC}-$Li_2C_4O_4$	AC + conducting carbon + CMC electrode incorporating dilithium squarate
Li-AC_{CMC}	AC + conducting carbon + CMC electrode incorporating dilithium squarate (same as AC_{CMC}-$Li_2C_4O_4$)
Li-AC-pristine	AC- $Li_2C_4O_4$ electrodes as prepared
Li-AC-2.5V	AC- $Li_2C_4O_4$ electrodes discharged to 2.5 V
Li-AC-1000-2.5V	AC- $Li_2C_4O_4$ electrodes after 1000 cycles, discharged to 2.5 V
Li-AC-4.2V	AC- $Li_2C_4O_4$ electrodes charged to 4.2 V
Li-AC_{CMC}-pristine	Li-AC_{CMC} electrodes as prepared
Li-AC_{CMC}-4V	Li-AC_{CMC} charged to 4 V
Li-AC_{CMC}-2.5V-$LiPF_6$	Li-AC_{CMC} discharged to 2.5 V and tested in 1 M $LiPF_6$ EC:DMC electrolyte
Li-AC_{CMC}-2.5V-$LiClO_4$	Li-AC_{CMC} discharged to 2.5 V and tested in 1 M $LiClO_4$ EC:DMC electrolyte

2.2. Surface Layer Characterization

To investigate the influence of $Li_2C_4O_4$ on the positive electrode surface, SEM was employed to examine the electrode morphology. Prior to electrode characterization, AC-$Li_2C_4O_4$ // HC full-cells were assembled and cycled for 10 cycles between 2 and 4.2 V at $C_{Li2C4O4}$/10 to ensure the complete decomposition of $Li_2C_4O_4$ and the pre-lithiation of the HC negative electrode. The GCD curves of the LIC during the $Li_2C_4O_4$ decomposition are presented in (Figure S1, Supporting Information). The selected electrolyte was 1 M $LiPF_6$ in EC : DMC (1 : 1 v/v), as it is the most commonly used electrolyte in LIC technology.[69,70]

SEM characterization was conducted on AC-$Li_2C_4O_4$ electrodes before electrochemical testing (Li-AC-pristine) and AC-$Li_2C_4O_4$ electrodes at 2.5 V *vs* Li^+/Li after $Li_2C_4O_4$ decomposition protocol (Li-AC-2.5V) **Figure 2**a presents the surface morphology of the Li-AC-pristine electrode before cycling. The larger particles correspond to AC, while the smaller particles belong to conductive carbon and the binder (PVdF in this case). $Li_2C_4O_4$ particles exhibit micrometric size (ca. 5 μm) and are not easily distinguishable from AC particles when only the morphology is being analyzed. As expected, no surface layer is observed on the electrode, as confirmed by the flat surface, sharp edges of AC particles, and the clear identification of the conductive carbon and binder components. In contrast, Figure 2b-d depicts the surface of Li-AC-2.5V, revealing a complete transformation in morphology after $Li_2C_4O_4$ decomposition, undoubtedly showing a surface layer on the electrode. This layer is formed during the $Li_2C_4O_4$ decomposition, possibly by the interaction of its decomposition products with both the electrode and the electrolyte. The surface layer completely covers the electrode, exhibiting an inhomogeneous porous structure as detailed in Figure 2d. However, this layer does not seem to block the pores of the AC in view of its electrochemical performance, allowing the ion exchange between the electrode surface and the electrolyte. In fact, it seems to be the origin of the observed increase in capacitance. Nevertheless, the formation of this surface layer could also be a sign of faster electrode degradation and does not by itself explain the electrochemical improvement. The chemical composition and stability of this surface layer seem to be of paramount importance to understand the behavior and properties of AC-based positive electrodes when $Li_2C_4O_4$ is integrated as a pre-lithiation agent.

To determine the chemical composition of the electrode surface layer and understand the influence of $Li_2C_4O_4$ on the positive electrode, XPS analysis has been carried out. XPS is able to detect and quantify the presence of all the elements present in the surface of the samples (with the exception of H and He) and determine their chemical environment.[46,47] Since the binding energy (BE) of core electrons can be obtained and it is sensitive to the

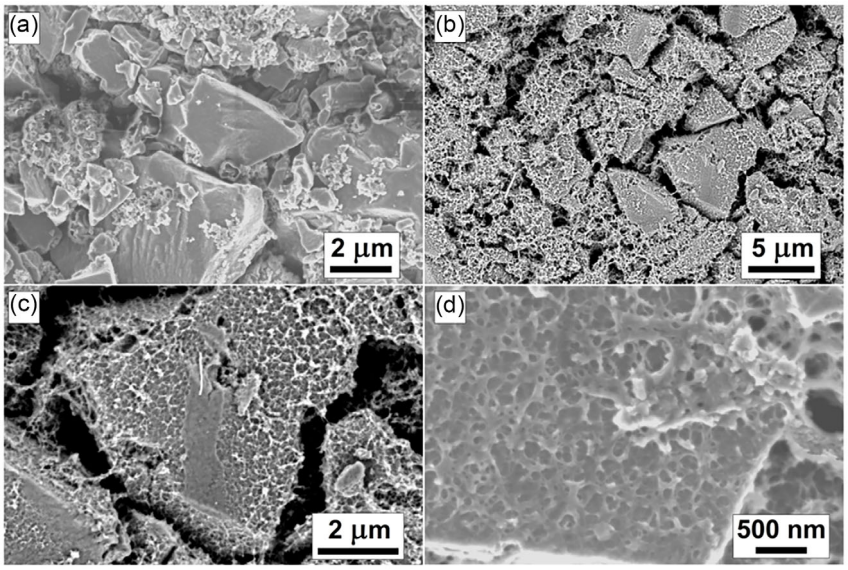

Figure 2. SEM images of a) Li-AC-pristine; b–d) Li-AC-2.5V at different magnifications.

local electronic density, not only the surface elemental composition can be calculated, but also the specific chemical compounds can be inferred by exploiting the chemical shift. The fact that only those photoelectrons emitted from close to the surface are able to escape without losing energy makes XPS a very surface-sensitive technique. Its probing depth is defined as the depth from which 95% of the photoelectron signal comes from, and it depends on the X-ray energy, the experimental geometry, the sample composition, and the measured core level.[48–50] In our case, the probing depth is ca. 10–15 nm. Thus, by knowing the XPS setup, analysis conditions, and chemical composition of the samples, the surface layer thickness can be estimated, provided its thickness is lower than the probing depth. To study the surface of AC-$Li_2C_4O_4$ electrodes, they were cycled for 10 cycles between 2.5 and 4.2 V versus Li^+/Li at 0.05 A g^{-1}.

Figure 3a-c illustrate the C 1s, O 1s and F 1s core levels of AC-$Li_2C_4O_4$ pristine (Li-AC-pristine), AC electrode at 4.2 V *vs* Li^+/Li after 10 cycles (AC-4.2V), AC electrode at 2.5 V versus Li^+/Li after 10 cycles (V), AC-$Li_2C_4O_4$ electrode at 4.2 V versus Li^+/Li after $Li_2C_4O_4$ decomposition protocol (Li-AC-4.2V), and AC-$Li_2C_4O_4$ electrode at 2.5 V *vs* Li^+/Li after $Li_2C_4O_4$ decomposition protocol (Li-AC-2.5V). The BE of all fitted peaks shown in this work are presented in Table S1-S5 (Supporting Information). As described in the experimental section, the AC-$Li_2C_4O_4$ pristine is composed of AC and C65, which only contain carbon with a slight proportion of oxygen; $Li_2C_4O_4$, composed of carbon, oxygen, and lithium; and PVdF, composed of carbon and fluorine. The components of the electrode also contain hydrogen, but since it is not detectable by XPS, it is not relevant in our analysis. Figure 3a depicts the C 1s spectrum of Li-AC-pristine, showing the typical chemical species found in carbonaceous electrodes. The peaks at 284.9 and 284.4 eV related to C—C/C—H and C═C chemical environments are identified for AC and C65 particles, composed almost entirely of carbon, which explains the high intensity of those peaks, especially the C═C one. The peaks fitted at 286.1 and 290.5 eV are related to the -$(CF_2$-C*$H_2)_n$- and -$(C^*F_2$-$CH_2)_n$- chemical environment of PVdF, respectively, while the component at 288.4 eV accounts for C═O and O—C═O bonds. Those moieties are essentially present in the $Li_2C_4O_4$ sacrificial salt, although some oxygenated groups can be attached to the AC surface during the AM synthesis and the electrode drying process. The O 1 spectrum of Li-AC-pristine has been fitted with two components at 533.4 and 531.2 eV, corresponding to C—O and C═O/CO_3/LiOH, respectively. As explained above, the oxygenated species present in the sample correspond to $Li_2C_4O_4$ and oxygen traces attached to the AC surface. Last, the F 1s spectrum of Li-AC-pristine is composed of two components at 687.6 and 689.8 eV related to -$(CF_2$-$CH_2)_n$- bonds of PVdF and some decomposition product (i.e., CF_3) or differential charging, respectively. The very few differences observed between Li-AC-pristine and AC-pristine are detailed in Figure S2 (Supporting Information), which is supported by the relevant information regarding the XPS analysis of those samples. The elemental composition of the different pristine samples is depicted in Figure S3 (Supporting Information)s, where the effect of the different binders and the integration of $Li_2C_4O_4$ in the chemical composition of the surface is clarified.

C 1s spectrum of AC-4.2V shown in Figure 3a displays many similarities with AC-$Li_2C_4O_4$ pristine (and AC-pristine), with the same chemical species and a similar amount of each one. Therefore, no surface layer or deposits have been formed. The main difference is the displacement of the C═C component to higher BE, as will be discussed later. The O 1s spectrum of AC-4.2V is illustrated in Figure 3b, which reveals the presence of C—O moieties at around 532.7 eV and two minor additional signals at 534.8 and 537.8 eV, corresponding to O-F/PO_x and differential charging. The O-F/PO_x component is related to the decomposition of the $LiPF_6$ and the solvent of the electrolyte, while differential charging is caused by the electrode inhomogeneities. Last, in the F 1s spectrum of AC-4.2V, the -$(CF_2$-$CH_2)_n$- signal decreases and a component at 686.5 eV appears,

Research Article
doi.org/10.1002/batt.202500495
Chemistry Europe
European Chemical Societies Publishing

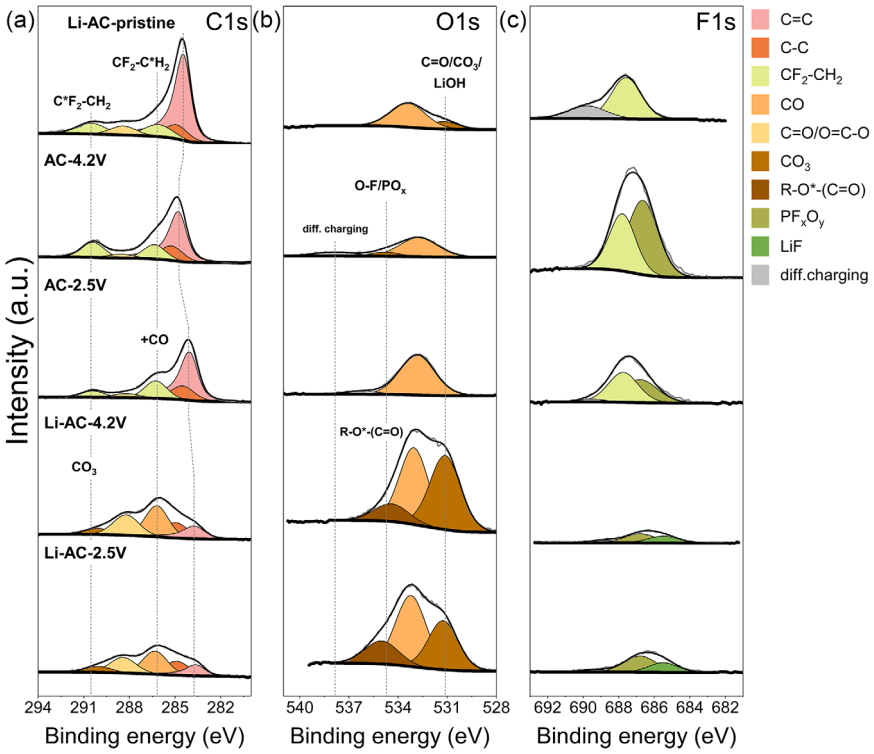

Figure 3. a) C 1s, b) O 1s, and c) F 1s XPS spectra of Li-AC-pristine; AC-4.2V; AC-2.5V; Li-AC-4.2V; and Li-AC-2.5V, from top to bottom.

corresponding to PF_xO_y, a decomposition product of the $LiPF_6$ salt whose presence denotes some electrolyte degradation. However, the high intensity of the -$(CF_2$-$CH_2)_n$- component of PVdF contradicts the presence of a thick layer on the electrode, as it was also concluded during the C 1s spectrum analysis. Few differences are found between AC-4.2V and AC-2.5V C 1s spectra. Only the component at 286.3 eV assigned to -$(CF_2$-$C^*H_2)_n$- seems to increase in AC-2.5V, due to the formation of C—O, which overlaps at a similar BE. In addition, the C═C component is shifted to lower BE. As for AC-4.2V, this behavior will be discussed later. As presumed from the C 1s spectrum, the only difference in the O 1s spectrum of AC-2.5V is a certain increase in the amount of C—O. The F 1s spectra of AC-2.5V show the same components, but with a lower amount of PF_xO_y, which may be redissolved into the electrolyte during cycling. Apart from the amount of C—O and PF_xO_y, almost no modifications have been found in the surface of the AC-based samples at different potentials, meaning that only some functional groups or deposits may be formed in the surface of the electrode. In addition, those deposits may form and dissolve into the electrolyte upon cycling.

Regarding the samples containing $Li_2C_4O_4$, the surface chemistry of the Li-AC-4.2V electrode is completely different from both AC-4.2V and Li-AC-pristine. In the C 1s spectrum, the C═C component almost disappeared, and it is further shifted down in BE to 283.7 eV. The signals corresponding to PVdF are no longer detected, indicating that a surface layer has been formed on top of the positive electrode, burying these bulk signals. While the intensity of the components related to the bulk electrode decreases, the amount of C═O/O═C—O bonds increases, a small amount of CO_3 is also detected at 290.0 eV, and the C—O (peaking at 286.2 eV) becomes the most abundant compound. Three components have been fitted in the O 1s spectrum of Li-AC-4.2V, corresponding to R-O*-(C═O), C—O, and C═O/CO_3/LiOH. The last component does not correspond to the $Li_2C_4O_4$ salt anymore, since it is decomposed during cycling; instead, those moieties are part of the surface layer that originates on top of the electrode. As expected from the C 1s fit, the amount of oxygen found in the Li-AC-4.2V sample is remarkably higher than in the AC-4.2V. In contrast to the Li-AC-pristine, AC-4.2V, and AC-2.5V samples, the -$(CF_2$-$CH_2)_n$- component of PVdF is absent from the F 1s spectrum of the Li-AC-4.2V electrode, which is essentially composed of PF_xO_y and LiF, though the fluorine content in this sample (and concretely PF_xO_y signal) is noticeably smaller than in the AC-4.2 and AC-2.5 samples. The chemical composition of Li-AC-2.5V is almost identical to Li-AC-4.2V. In the C 1s spectra, only a slight decrease in the amount of C—O, C═O/O═C—O, and CO_3 is observed, as confirmed by their respective reduction in O 1s. At low potential, those compounds may partially redissolve into the electrolyte. Last, few differences exist between Li-AC-2.5V and Li-AC-4.2V F 1s spectra, just with a slight increase of fluorine signal for AC-2.5V. The P 2p and Li 1 sin spectra of AC-4.2V, AC-2.5V, Li-AC-4.2V, and Li-AC-2.5V are depicted in Figure S4, Supporting Information, accompanied by the samples analysis and comparison, where very small phosphorus content and noticeable lithium amount are seen in Li-AC electrodes in contrast to AC ones.

As mentioned above, the disappearance of the C═C, -$(CF_2$-$C^*H_2)_n$- and -$(C^*F_2$-$CH_2)_n$- components from the C 1s and the -$(CF_2$-$CH_2)_n$- component from the F 1s spectra can be explained

Research Article
doi.org/10.1002/batt.202500495
Chemistry Europe
European Chemical Societies Publishing

by the growth of a surface layer on top of the electrode. The surface layer is thick enough to prevent the photoelectrons originating in the bulk electrode (carbon and PVdF) from escaping through it, thus, the signal of the bulk electrode cannot be detected.

The elemental composition of AC-pristine, AC-4.2V, AC-2.5V, Li-AC-pristine, Li-AC-4.2V, and Li-AC-2.5V is presented in **Figure 4**. As clearly seen, the differences between pristine and cycled electrodes are much more pronounced for the Li-AC samples due to surface layer formation. In the case of samples without $Li_2C_4O_4$, from 4.2 to 2.5 V, the amount of carbon and especially oxygen increases, and the amount of fluorine decreases. As observed in the XPS spectra, the differences are less remarkable between Li-AC-4.2V and Li-AC-2.5V. Moreover, in contrast to the previous trend, oxygen slightly decreases while fluorine increases from 4.2 to 2.5 V, together with a slight reduction in the proportion of lithium.

As commented above, a BE shift is observed between the C═C component of the different samples analyzed in Figure 3. Such a shift may have its origin in several phenomena: i) The formation of an insulating SEI or surface layer rich in Li^+ polar species has been reported to induce an electric potential gradient at the buried electrode-surface layer interface.[51–53] In this case, the BE shift is not caused by differential charging nor by chemical changes in the SEI/electrode, but by the accumulation of charges at the electrode-surface layer interface, resulting in a shift to lower BE values of the bulk electrode species with respect to the surface layer components. The electric potential gradient has been observed to depend on the state-of-charge of the electrode, which correlates with the electrode potential; and it is also affected by the surface layer properties (i.e., thickness and electrical conductivity). ii) Chemical changes or chemisorption on the samples' surfaces usually induce changes in the local electronic structure of the materials, modifying certain properties of the material such as the electrical conductivity. Thus, changes in the electrode potential led to the interaction between the electrode surface and certain chemical species, triggering adsorption/desorption. Depending on the electronegativity of the adsorbed species, electron donation/withdrawal between the adsorbate and the underlying electrode may occur,[54,55] modifying the electrode surface BE with respect to the uncharged sample.

Unfortunately, most of the studies reporting this effect are based on the negative electrode of lithium-ion batteries (LIBs) whose charge storage mechanism is based on the lithiation and delithiation of the AM. This electrochemical mechanism allows the direct correlation between high-density of charges (lithiated) and low-density of charges (delithiated) at the interface. However, in the case of AC positive electrodes used in LICs, which adsorb ions during charge (PF_6^-) and during discharge (Li^+), this relation is not so clear, and the BE shift cannot be correlated uniquely and unequivocally to the accumulation of charges in the interface. The formation of a Li^+ containing surface layer in cycled Li-AC electrodes may result in a similar scenario to that of LIBs electrodes, and in this case, the permanent dipole between the electrode and the surface layer always results in a shift of the C═C peak to lower BE. By contrast, the nature of the adsorbed ions (cations or anions) and their different electronegativity seem to have a higher influence for AC-4.2 and AC-2.5 electrodes, showing positive or negative BE shifts of the C═C signal depending on the polarization. In any case, more in-depth studies are needed to provide a full explanation of these phenomena in AC electrodes used in LICs.

Thus, the XPS analysis has demonstrated the unexpected formation of a surface layer on the electrodes, including $Li_2C_4O_4$. The surface layer is mainly formed by oxygenated species, as C-O, C═O/O─C=O, and LiOH due to the action of the Li^+, CO_2, and CO released during salt decomposition. The surprising formation of a functional surface layer on the positive electrode is controversial, since most of the literature regarding AC electrodes considers the formation of deposits on the surface as part of the degradation mechanism of the devices.[56–58] Those deposits

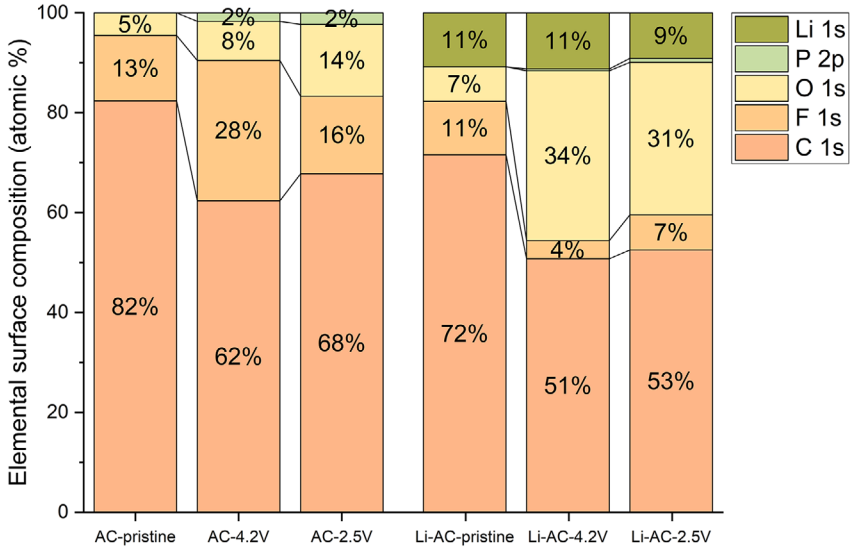

Figure 4. Elemental surface composition (at. %) of AC-pristine; AC-4.2V; AC-2.5V; Li-AC-pristine; Li-AC-4.2V; and Li-AC-2.5V obtained from the XPS analysis.

may increase the resistance of the electrode and block the pores, dramatically reducing the capacity. To the best of our knowledge, only one study regarding functional surface layers on AC positive electrodes has been reported. Shen et al.[59] studied an AC // AC asymmetric cell using 1 M $TEABF_4$ in PC, where an electrode potential above the decomposition potential of PC was applied. This led to functionalizing the AC surface by the decomposition by-products of PC (CO_2 among them). The functionalization protocol consisted of 5 repetitions of 100 cycles using fresh electrolyte, which ultimately hindered the scale-up of this functionalization strategy. Furthermore, the chemical composition of the layer is unknown, impeding the understanding of the occurring phenomena.

Furthermore, the evolution of the surface layer composition during charge and discharge has also been analyzed, resulting in a high stability without significant modifications, independently of the applied potential. The surface layer formed on the electrode must be responsible for the electrochemical performance enhancement, contributing to the energy storage through pseudocapacitive mechanisms. Indeed, as described in the Introduction, oxygenated species are related to pseudocapacitance, especially in aqueous[25] but also in organic electrolytes.[59]

2.3. Surface Layer Stability

The previous section described the surface layer characteristics and their impact on the electrochemical performance of AC positive electrodes. The significance of these characteristics lies in their stability over cycling; otherwise, they could be considered as mere by-products of side reactions occurring during formation cycles rather than an electrode functionalization.

The electrochemical behavior of the AC and AC-$Li_2C_4O_4$ positive electrodes has been analyzed in a half-cell configuration to avoid any contribution of the HC negative electrode. The characterization consisted of a cyclability test at 1 A g^{-1} between 2 and 4.2 V *vs* Li^+/Li, with five control CV cycles every 200 cycles recorded at 5 mV s^{-1} between 2 and 4.2 V versus Li^+/Li. **Figure 5**a shows the evolution of the specific capacity of AC-$Li_2C_4O_4$ and AC over 6500 cycles. At 1 A g^{-1}, the initial capacity of AC-$Li_2C_4O_4$ and AC are 74.2 and 53 mAh g^{-1}, respectively. During the aging test, the capacity decreases progressively due to the degradation of the cell elements. The AC-$Li_2C_4O_4$ capacity reaches 80% of the original value after 6000 cycles, marked in Figure 5a with a gray dashed line at 59.3 mAh g^{-1}. After 6500 cycles, the capacity of AC-$Li_2C_4O_4$ is 57.0 mAh g^{-1}, still higher than the initial capacity of AC. That observation is in alignment with the presence of the surface layer after long cycling experiments, which, after 6500 cycles, continues to contribute to the total capacity of the electrode. If the surface layer had dissolved and disappeared during the cycling test, the capacity of AC-$Li_2C_4O_4$ would have dropped to a value similar to that of AC.

In addition, Figure 5b,c shows GCD curves and CVs of AC-$Li_2C_4O_4$, respectively, after 200, 2000, 4400, and 6500 cycles. In Figure 5b the GCD curves maintain the triangular shape throughout the cyclability test; however, the ohmic drop progressively increases with the number of cycles, indicating a rise in resistance. The increase in resistance could be caused by several factors, such as electrolyte degradation, AC dissolution, delamination, pore blocking, or surface layer modification. The increase in resistance is also evidenced by the loss of the quadratic shape of the CVs over cycling (Figure 5c). However, an unexpected second phenomenon can also be observed: the shape of the CVs changes over the cycling test. While the area of the CV below the open circuit voltage (OCV) (≈3 V *vs* Li^+/Li) decreases, the area above the OCV increases. This behavior could be related to the thickening of the surface layer, which weakens the capacitive mechanism while favoring the pseudocapacitive one. This competition between capacitive and pseudocapacitive mechanisms has important consequences in LICs, since it could maintain a high-capacity retention, but it may also impact the potential swing of the positive electrode. This could turn into some negative consequences, such as higher electrolyte degradation if the upper potential increases, or the modification of the negative electrode swing, which might lead to lithium plating. Nevertheless, those consequences are multifactorial and can be critically affected by the mass balance, mass ratio, electrode surface, total energy, or final device configuration (e.g., coin, Swagelok, or pouch cell), among others. Hence, further research is necessary to fully understand the electrochemical consequences of the surface layer formed on top of the AC positive electrode, which is beyond the scope of this work.

To further analyze the stability of the surface layer, a LIC composed of an AC-$Li_2C_4O_4$ positive electrode and an HC

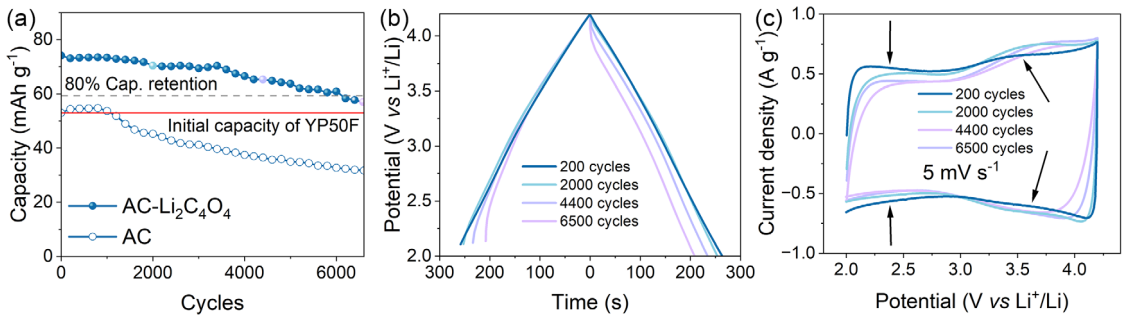

Figure 5. a) Cyclability test of Li-AC and AC at 1 A g^{-1} between 2 and 4.2 V versus Li^+/Li; b) GCD of Li-AC during the cyclability test; and c) CVs of Li-AC during the cyclability test.

negative electrode was assembled. After the pre-lithiation step, AC-$Li_2C_4O_4$ // HC cells were cycled for 1000 cycles at 1 A g^{-1} between 2 and 4.2 V, retaining 93% of the initial capacity. After 1000 cycles, the positive electrode was characterized by XPS to confirm the presence of the surface layer and the continuity of its chemical composition. **Figure 6** shows the C 1s, O 1s, and F 1s of Li-AC-2.5V and the AC-$Li_2C_4O_4$ electrode at 2.5 V versus Li^+/Li after 1000 cycles (Li-AC-1000−2.5 V). After 1000 cycles, the surface layer undoubtedly remains on the electrode, as can be confirmed by the strong decrease of the buried C═C signal and absence of PVdF components in both C 1s and F 1s spectra. Besides, the chemical composition of the surface layer of Li-AC-1000−2.5 V maintains a lot of similarities with that of Li-AC-2.5V. The C 1s spectra show the same chemical species in both samples, though the amount of CO and C═O/COO increases after the 1000-cycles test, as confirmed by the increase in all components in the O 1s spectrum. Similarly, F 1s spectra show the same components but with an increase in PF_xO_y and LiF content. Some traces of PF_6 might be present in the sample, contributing to increasing the signal attributed to PF_xO_y. Thus, it seems that the surface layer roughly maintains its composition except for the rising amount of fluorinated compounds, formed from $LiPF_6$ salt decomposition. The P 2p and Li 1s spectra of Li-AC-2.5V and Li-AC-1000-2.5V electrodes are presented in Figure S5, Supporting Information, whose analysis is also detailed there. The modifications in the chemical composition allow identifying the $LiPF_6$ decomposition and the formation of PF_xO_y and LiF as the main result of the aging test on the electrode surface.

Figure S6 (Supporting Information) depicts the elemental composition of Li-AC-2.5V and Li-AC-1000-2.5V electrodes. When the elemental compositions of Li-AC-2.5V and Li-AC-1000-2.5V are compared, a small increment in the amount of fluorine is found after the 1000-cycles test, corresponding to the higher electrolyte decomposition and concretely the PF_xO_y and LiF increase. The change in the surface layer composition might be the reason for the increased resistance over time. The amount of carbon and lithium has therefore been minimally reduced, signaling the high level of stability of the surface layer. Thus, as stated above, the decomposition of $Li_2C_4O_4$ triggers the formation of a surface layer rich in oxygen whose composition is maintained after 1000 cycles.

2.4. Unraveling Surface Layer Formation

The formation of the surface layer on the positive electrode is associated with the reaction of the $Li_2C_4O_4$ decomposition products (Li^+, CO_2. and CO) with the different components of the cell. Among them, the highly reactive fluorinated compounds are ideal candidates for decomposing and for catalyzing electrolyte decomposition, leading to the surface layer formation. The fluorinated components of the cells are the PVdF binder and the $LiPF_6$ salt. Thus, to confirm the role of fluorine in the surface layer formation, a fluorine-free system was fabricated. In this system, AC-$Li_2C_4O_4$ and AC electrodes were fabricated, replacing PVdF binder with carboxymethyl cellulose (CMC), and the 1 M $LiPF_6$ in EC : DMC electrolyte with 1 M $LiClO_4$ in EC : DMC. The electrochemical characterization of the fluorine-free system was performed in a half-cell configuration since the use of $Li_2C_4O_4$ as a pre-lithiation agent has not been optimized for this system. The cell was cycled between 2 and 4 V versus Li^+/Li to avoid Al foil corrosion, which takes place in $LiClO_4$-based electrolytes above 4 V versus Li^+/Li. **Figure 7**a shows the GCD of AC-$Li_2C_4O_4$ with CMC (hereafter named as Li-AC_{CMC}) during the $Li_2C_4O_4$ decomposition protocol. Figure 7b shows the GCD of Li-AC_{CMC} and AC with CMC (hereafter named AC_{CMC}) at 3 A g^{-1}. In contrast with the performance of Li-AC and AC observed in Figure 1, Li-AC_{CMC} and AC_{CMC} show a very similar behavior (actually, AC_{CMC} provided slightly larger discharge times). However, both electrodes performed as expected, showing the triangular shape characteristic of capacitive systems. In good agreement, the CVs of Li-AC_{CMC} and AC_{CMC} presented in Figure 7c are almost identical. The similarities between the two fluorine-free systems are confirmed in Figure 7d, which shows the very similar rate capability of those samples. Figure 7e shows a lower resistance for the Li-AC_{CMC} sample, which is also in contrast with respect to the fluorinated case. The comparable electrochemical performance of both fluorine-free samples confirms our hypothesis of fluorine being the main contributor to the performance enhancement for Li-AC.

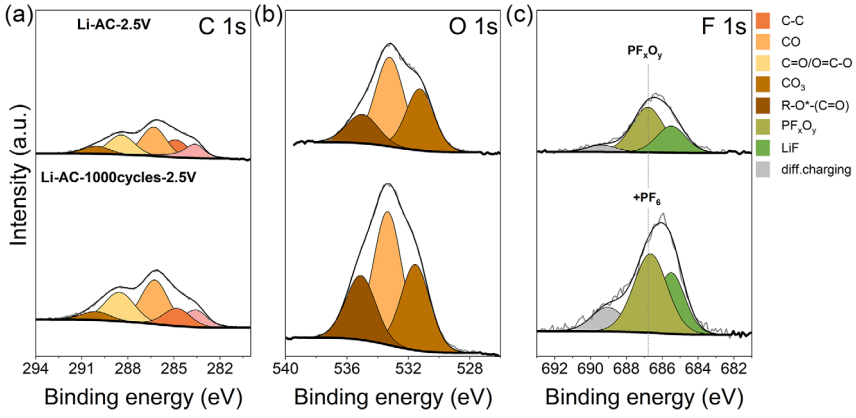

Figure 6. a) C 1s, b) O 1s, and c) F 1s XP spectra of Li-AC-2.5V; and Li-AC-1000cycles-2.5V, from top to bottom.

Research Article
doi.org/10.1002/batt.202500495
Chemistry Europe
European Chemical Societies Publishing

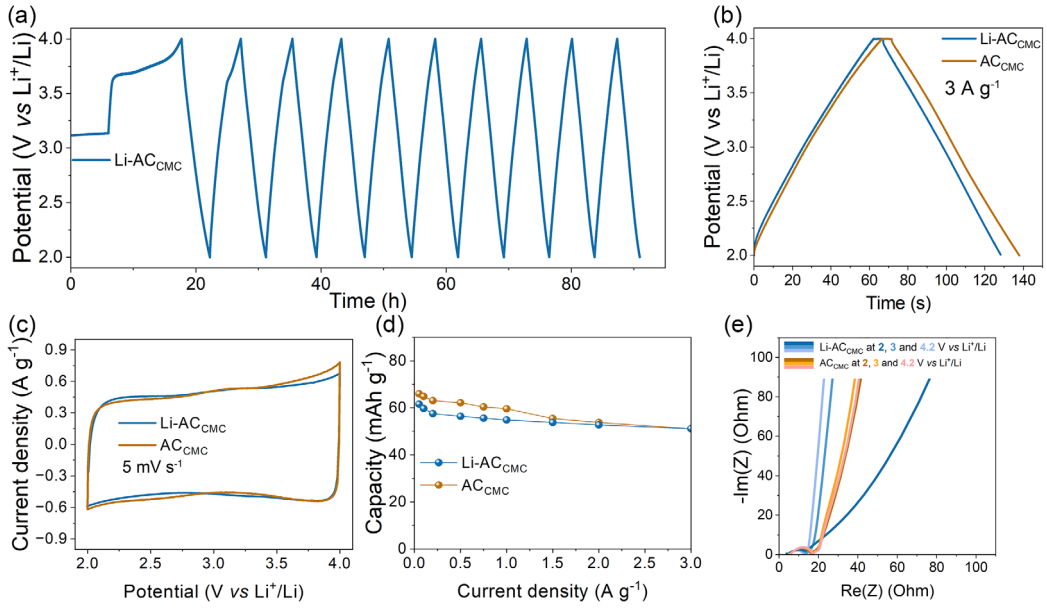

Figure 7. Electrochemical characterization of Li-AC_{CMC} (blue) and AC_{CMC} (brown) using 1 M $LiClO_4$ in EC : DMC: GCD during the $Li_2C_4O_4$ decomposition protocol; a) decomposition protocol during first GCD cycles b) GCD curves at 3 A g^{-1}; c) CV at 5 mV s^{-1}; d) rate capability between 0.05 and 3 A g^{-1}; and e) PEIS at 2.0, 3.0 and 4.0 V versus Li^+/Li.

Since the electrochemical improvement in the system containing fluorine has been associated with the formation of a surface layer, the surface of the Li-AC_{CMC} electrodes has been characterized by SEM for comparison. AC_{CMC}-$Li_2C_4O_4$ samples at 2.5 V *vs* Li^+/Li after the $Li_2C_4O_4$ decomposition protocol (Li-AC_{CMC}—2.5 V) were characterized by SEM as shown in Figure S7 (Supporting Information). In this case, no surface layer is observed on the electrode, and the different components of the electrode (i.e., AC, conductive carbon, and binder CMC in this case) can be easily identified. Therefore, the AC particles exhibit flat surfaces with no visible deposits, similarly to what is observed for Li-AC-pristine depicted in Figure 2a. The absence of the surface layer correlates well with the similar electrochemical performance of AC_{CMC} and Li-AC_{CMC}, further confirming the active role of the surface layer in the charge storage process.

Therefore, the fluorine-free electrodes were analyzed by XPS to disclose the chemical composition of the surface, understand the changes that occurred on the surface after the $Li_2C_4O_4$ decomposition, and ascertain the differences with respect to electrodes containing fluorine. The C 1s, O 1, and F 1s spectra of the fluorine-free electrode before cycling (named as Li-AC_{CMC}-pristine) show some differences with respect to the electrodes using PVdF as binder, as evidenced in Figures S2 and S3 (Supporting Information). In the C 1s spectrum, the -$(C^*F_2\text{-}CH_2)_n$- and -$(CF_2\text{-}C^*H_2)_n$- components of PVdF are obviously not present in the fluorine-free electrode, while the CO component, due to the CMC binder, increases in size and its BE is slightly modified. The CO_3 signal present in the sample might be the result of certain degradation of the CMC or the $Li_2C_4O_4$ during the fabrication of the electrode. The O 1s spectrum of Li-AC_{CMC}-pristine includes the same components present in Li-AC-pristine, with a new component ascribed to the Na Auger signal. Last, the F 1s spectrum confirms the absence of fluorine in the Li-AC_{CMC}-pristine sample.

Then, fluorine-free electrodes were analyzed at 4 V versus Li^+/Li after the $Li_2C_4O_4$ decomposition protocol (i.e., 10 cycles between 2.5 and 4 V versus Li^+/Li at $C_{Li2C4O4}/10$) using 1 M $LiClO_4$ in EC : DMC. **Figure 8** compares the XPS spectra of Li-AC_{CMC}-pristine and Li-AC_{CMC} at 4 V versus Li^+/Li after the $Li_2C_4O_4$ decomposition protocol using 1 M $LiClO_4$ in EC : DMC as electrolyte (hereafter named Li-AC_{CMC}-4 V). As a visual reference, the previously analyzed Li-AC-4.2V sample has been included in Figure 8. The C 1s spectra show few differences between Li-AC_{CMC}-pristine and Li-AC_{CMC}-4 V. Same components have been found in both electrodes, which are characterized by a large C═C component corresponding to the AC AM. After the $Li_2C_4O_4$ decomposition, the amount of CVO/O═C—O and CO decreases because the $Li_2C_4O_4$, which includes those chemical bonds, is not present in the sample anymore. Comparable amounts of CO_3 have been found in the Li-AC_{CMC}-pristine and Li-AC_{CMC}-4 V, indicating that after cycling, no more carbonates are formed at the surface. In the case of O 1s spectra, Li-AC_{CMC}-4 V shows the same components as Li-AC_{CMC}-pristine, but with a lower amount of C—O due to $Li_2C_4O_4$ salt decomposition. In the case of F 1s spectra, both Li-AC_{CMC}-pristine and Li-AC_{CMC}-4 V samples showed a total absence of fluorine. Thus, the surface composition of Li-AC_{CMC}-4 V is similar to that of Li-AC_{CMC}-pristine, and completely different from Li-AC-4.2V one. Contrary to the case of Li-AC-4.2V, no surface layer is formed on the Li-AC_{CMC}-4 V electrode, confirming the role of the $Li_2C_4O_4$-fluorine interaction in the surface layer formation.

The surface elemental compositions of Li-AC_{CMC}-pristine and Li-AC_{CMC}-4 V are depicted in Figure S8 (Supporting Information). Li-AC-pristine and Li-AC-4.2V are also included as a reference.

Research Article
doi.org/10.1002/batt.202500495
Chemistry Europe
European Chemical Societies Publishing

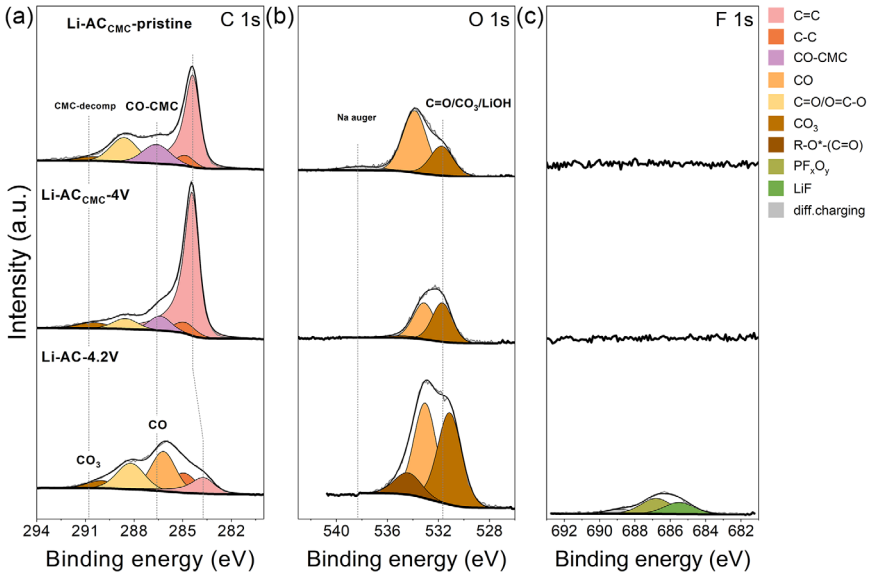

Figure 8. a) C 1s, b) O 1s, and c) F 1s XPS spectra of Li-AC$_{CMC}$-pristine; Li-AC$_{CMC}$-4 V; and Li-AC-4.2V, from top to bottom.

The surface elemental composition clearly illustrates the formation (or absence) of a surface layer in the electrodes. The decomposition of $Li_2C_4O_4$ integrated in Li-AC$_{CMC}$-pristine does not form a surface layer on the electrode. In consequence, the lithium has completely disappeared in the Li-AC$_{CMC}$-4 V sample, while the amount of oxygen decreases, since they form part of the $Li_2C_4O_4$. The amount of carbon increases, and a small amount of chlorine appears as it is deposited on the electrode. On the other hand, the oxygen-rich surface layer formed on the Li-AC-4.2V samples completely modifies the elemental composition of the surface. Thus, the relation of fluorine with the surface layer formation and the electrochemical performance enhancement has been demonstrated. However, initially, two sources of fluorine were present in the system: the PVdF binder and the $LiPF_6$ salt. To isolate the contribution of those two components, a fluorine-free electrode (Li-AC$_{CMC}$) was cycled in 1 M $LiPF_6$ in EC : DMC for 10 cycles between 2.5 and 4.2 V versus Li^+/Li to decompose the $Li_2C_4O_4$. The cycling was stopped at 2.5 V *vs* Li^+/Li, and the electrode was characterized by XPS (hereafter named as Li-AC$_{CMC}$-2.5 V-$LiPF_6$). Hence, **Figure 9** shows the XPS spectra of Li-AC$_{CMC}$—2.5 V-$LiPF_6$ and Li-AC$_{CMC}$-2.5 V-$LiClO_4$. Li-AC-2.5V has been included in Figure 9 as a visual reference to enable the comparison between the different systems. Li-AC$_{CMC}$—2.5 V-$LiClO_4$ sample corresponds to AC electrodes containing $Li_2C_4O_4$ and CMC, which have been cycled using 1 M $LiClO_4$ in EC : DMC electrolyte to decompose the $Li_2C_4O_4$. The cycling was stopped at 2.5 V versus Li^+/Li prior to XPS analysis. The C 1s spectra of Li-AC$_{CMC}$—2.5 V-$LiPF_6$ confirm that the surface layer is formed, although no PVdF is present in the electrode, since the intensity of the component assigned to C═C significantly decreases. The surface composition is different from that of Li-AC-2.5V due to the presence of CMC and its decomposition products instead of PVdF. Nevertheless, the composition differs very little, indicating that $LiPF_6$ is the main contributing factor to the surface layer formed on AC. In the case of Li-AC$_{CMC}$—2.5 V-$LiClO_4$, as previously observed for Li-AC$_{CMC}$-4 V -cycled using 1 M $LiClO_4$ in EC : DMC electrolyte-, no surface layer is formed on the electrode and the C═C component of the bulk electrode is perfectly visible. Nevertheless, the component corresponding to CO_3 increased, revealing the formation of carbonates during cycling. Those carbonate deposits allow the detection of the bulk electrode because they are either isolated and do not form a homogeneous layer, or they only form a very thin layer with a thickness significantly lower than the XPS information depth. Moreover, since they are not observed in Li-AC$_{CMC}$-4 V, we can assume that they form and dissolve during cycling. Similar behavior has been observed in AC$_{CMC}$ electrodes when $Li_2C_4O_4$ is not used, confirming that this effect is not related to the action of the $Li_2C_4O_4$ (see Figure S9, Supporting Information). The O 1s spectrum of Li-AC$_{CMC}$—2.5 V-$LiPF_6$ shows a high amount of C═O/CO_3/LiOH, which might appear as a decomposition product of CMC in the 1 M $LiPF_6$ EC : DMC electrolyte.[60] Li-AC$_{CMC}$—2.5 V-$LiClO_4$ sample contains mainly CO from the CMC binder and carbonates, in agreement with the C 1s spectrum. The F 1s spectra of Li-AC$_{CMC}$—2.5 V-$LiPF_6$ exhibit a comparable composition to that of the Li-AC-2.5V sample, suggesting that the fluorinated species observed in Li-AC-2.5V are predominantly derived from $LiPF_6$ and not PVdF.

To conclude, the elemental surface compositions of Li-AC-2.5V, Li-AC$_{CMC}$-2.5 V-$LiPF_6$ and Li-AC$_{CMC}$-2.5V-$LiClO_4$ are shown in Figure S10, Supporting Information. Similar chemical species and elemental composition have been found in Li-AC-2.5V and Li-AC$_{CMC}$-2.5V-$LiPF_6$. However, lower content of fluorine and oxygen is present at the surface of the Li-AC$_{CMC}$-2.5V-$LiPF_6$ sample, with a higher amount of lithium. The elemental surface composition of Li-AC$_{CMC}$-2.5V-$LiPF_6$ and Li-AC$_{CMC}$-2.5V-$LiClO_4$ surprisingly result in being very similar. Nevertheless, as commented during the XPS spectra analysis, the chemical compounds at the surface are very different. Both contain a high amount of O, which in the first case corresponds to an oxygen-rich surface layer, while in the second case corresponds to the CMC binder in the electrode

Research Article
doi.org/10.1002/batt.202500495
Chemistry Europe
European Chemical Societies Publishing

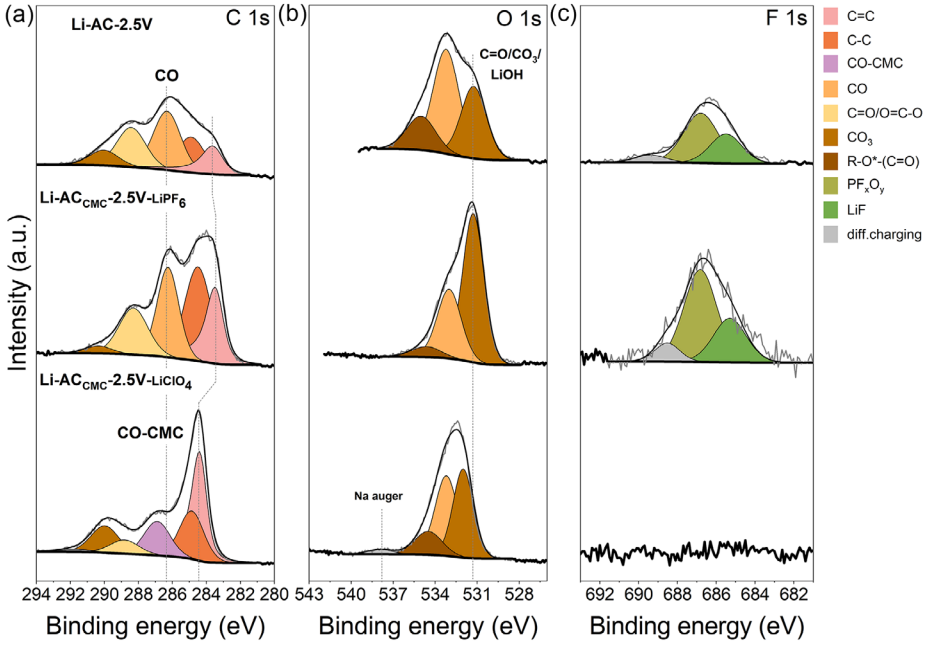

Figure 9. a) C 1s, b) O 1s, and c) F 1s XPS spectra of Li-AC-2.5V; Li-AC$_{CMC}$-2.5 V-LiPF$_6$ and Li-AC$_{CMC}$-2.5 V-LiClO$_4$, from top to bottom.

(here visible because of the lack of a burying layer on top) and the formation of surface carbonates.

Those results confirm that, although the surface analysis reveals the presence of slightly different chemical composition, the surface layer is undoubtedly formed when CMC is used as a binder if the electrolyte contains LiPF$_6$ salt. Hence, it can be concluded that, although the binder impacts the surface layer composition, it does not play a critical role in its formation. Indeed, the LiPF$_6$ salt used in the electrolyte is the main contributor to the surface layer formation, together with the $Li_2C_4O_4$ sacrificial salt. LiPF$_6$ salt may react with CO_2 and CO formed during $Li_2C_4O_4$ decomposition, leading to the formation of different compounds. The fluorinated compounds resulting from the LiPF$_6$ decomposition could also catalyze the solvents' decomposition, leading to the precipitation of oxygenated compounds that might enhance the capacity and rate capability of the AC electrodes through pseudocapacitive mechanisms, improving the overall electrode performance. Interestingly, all of this does not seem to affect the durability of the system, as it has been demonstrated that it can withstand a floating test of over 1500 h at 50 °C.[61,62]

Moreover, this mechanism could explain the modification of the SEI on the negative electrode that has been previously reported when $Li_2C_4O_4$ is used together with 1 M LiPF$_6$ EC : DMC electrolyte. Thus, understanding the role of LiPF$_6$ in the surface layer formation might lead to improvements in cell stability and the fabrication of artificial SEIs and surface layers in both the negative and positive electrodes. Last, more investigations are needed to identify if the combination of other fluorinated salts (e.g., LiTFSI[63] or LiBF$_4$), sacrificial salts (e.g., $Li_2C_2O_4$[64] or $Na_2C_4O_4$[65]), or solvents (e.g., PC, CPAME[66] or GVL[67]) might lead to similar consequences, enabling the extension of this finding to new systems with alternative electrolytes.

3. Conclusions

This study demonstrates that using $Li_2C_4O_4$ as a pre-lithiation agent in LICs not only compensates for lithium loss at the negative electrode but also improves the electrochemical performance of the AC positive electrode. The enhanced capacity and rate capability are attributed to the formation of a stable surface layer, whose composition and role have been elucidated through complementary analyses. The results suggest that the combination of $Li_2C_4O_4$ with fluorinated components in the electrolyte plays a key role in surface layer formation, offering new insights into interfacial engineering strategies for high-performance LICs. These findings highlight the dual function of $Li_2C_4O_4$—both as a lithium donor and as a promoter of surface modifications beneficial to pseudocapacitive behavior. Overall, this work contributes to a deeper understanding of sacrificial salt chemistry and provides a foundation for the design of next-generation pre-lithiation strategies that enhance performance, stability, and versatility in LICs and related energy storage systems.

4. Experimental Section

Electrode Fabrication

AC-$Li_2C_4O_4$ positive electrodes were prepared by dispersing in N-methyl-2-pyrrolidinone (NMP, Merck) a commercial AC (YP-50F, Kuraray), dilithium squarate ($Li_2C_4O_4$), Super C65 conductive carbon (Imerys, C-NERGY), and polyvinylidene fluoride (PVdF, Solef) in a mass ratio of 63.5 : 27 : 5 : 4.5. $Li_2C_4O_4$ sacrificial salt was synthesized as reported elsewhere[6] and included as the pre-lithiation additive. AC electrodes were fabricated by analogous methods by dispersing in NMP a mixture of AC, Super C65, and PVdF using a 90 : 5 : 5 mass ratio.

Moreover, fluorine-free electrodes (AC_{CMC}-$Li_2C_4O_4$) were fabricated by dispersing AC, dilithium squarate, Super C65, and CMC using a mass ratio of 63.5 : 27 : 5 : 4.5 in a mixture of water and ethanol (70 : 30 vol.). AC_{CMC} electrodes were also fabricated by dispersing AC, Super C65 and CMC in an ethanol : water mixture (70 :30 v/v), using a 90 : 5 : 5 mass ratio. Then, the dispersions were vigorously stirred, and the slurries were coated onto aluminum foil.

Negative electrodes based on HC (Kuraray), Super C65, and PVdF were fabricated by dispersing the components into NMP with a 90 : 5 : 5 mass ratio, and the slurry was coated onto copper foil. Laminates were dried at 80 °C for 12 h under vacuum.

Electrode discs of 12 mm were punched out of the AC- and HC-based laminates and dried at 120 °C overnight under vacuum prior to cell assembly.

Self-standing AC electrodes were fabricated by mixing AC, Super C65, and polytetrafluoroethylene (PTFE) using a 85 : 10 : 5 mass ratio with water and ethanol in 30 : 70 volumetric ratio. The electrodes were dried at room temperature and then at 120 °C overnight under vacuum prior to cell assembly.

Physicochemical Characterization

The morphology of the samples was characterized by SEM using an APREO 2 S HiVac microscope. The measurements were performed using a low acceleration voltage of 2 kV, which facilitated the observation of elements of the surface. Composition and topography information were combined in the images.

XPS were recorded using two different systems. Most of the spectra were collected in a Phoibos 150 XPS spectrometer (SPECS Surface Nano Analysis) installed in an ultra high vacuum (UHV) chamber with a base pressure of 5×10^{-10} mbar employing a non-monochromatic Mg source (Kα with h$\nu = 1253.6$ eV). The survey spectra were recorded using $E_{step} = 0.5$ eV and $E_{pass} = 90$ eV, while the high-resolution regions of the different elements were recorded employing $E_{step} = 0.1$ eV and $E_{pass} = 30$ eV.

In addition, a PHI5000 VersaProbe III Scanning X-ray Microprobe XPS system (ULVAC-PHI, Inc.) with a monochromatic Al source (h$\nu = 1486.6$ eV) was also employed for the measurements of samples containing CMC binder (i.e., Li-AC_{CMC}-pristine, Li-AC_{CMC}-4V, Li-AC_{CMC}-2.5V, AC_{CMC}-4V, AC_{CMC}-2.5V-$LiClO_4$, and Li-AC_{CMC}-2.5V-$LiPF_6$). For survey spectra, a step size of 0.25 eV and a pass energy of 140 eV were used, while high-resolution spectra of the different elements were recorded using $E_{step} = 0.1$ eV and $E_{pass} = 55$ eV.

Prior to the XPS measurements, the electrodes were recovered from the cells and cleaned with DMC to remove excess electrolyte and separator traces that could be deposited on them. The cells were disassembled, and the electrodes were cleaned inside a glovebox under an inert Ar atmosphere. Then, the electrodes were mounted on a sample holder and transferred to the spectrometer using an inert transport vessel to avoid any contact with the air and preserve the SEI unaltered. CASA XPS software was employed for data analysis.[68] In the cycled samples, the BE scale was referenced to the hydrocarbon bond at 284.8 eV and refined using other peaks, since this one was not very intense nor isolated. To model the photoelectron peaks, Voigt functions (70% Gaussian, 30% Lorentzian) were used for all photoelectron peaks except for semi-metallic sp^2 C═C, where an asymmetric pseudo-Voigt (APV) function was considered.[19,69] A Shirley-type background was employed to remove the inelastically scattered photoelectron signal.

Electrochemical Characterization

The GCD, CV, and potentiostatic EIS (PEIS) measurements were performed in a VMP3 generator from Biologic. In GCD, during both charge and discharge, the same current density is applied with a 5 s rest step. Thus, the electrochemical performance of the positive electrode was evaluated by using 3-electrode Swagelok cells in half-cell configuration, with AC-based working electrode (i.e., AC-$Li_2C_4O_4$, AC, AC_{CMC}-$Li_2C_4O_4$, and AC_{CMC}), self-standing AC counter electrode, and Li metal reference electrode. The self-standing AC counter electrode was oversized, thus only a small fraction of its total capacity was used, limiting its influence on the overall half-cell performance. While AC and AC-$Li_2C_4O_4$ electrodes were characterized between 2 and 4.2 V *vs* Li^+/Li, AC_{CMC} and AC_{CMC}-$Li_2C_4O_4$ were characterized between 2 and 4 V versus Li^+/Li to avoid aluminum current collector corrosion in 1 M $LiClO_4$ EC : DMC electrolyte. The cells containing $Li_2C_4O_4$ followed a cycling protocol consisting of 10 GCD cycles between 2 and 4.2 V versus Li^+/Li (2—4 V *vs* Li^+/Li in the case of cells containing $LiClO_4$-based electrolyte) at $C_{Li2C4O4}$/10 (defining $C_{Li2C4O4} = 425$ mAh g^{-1}) to ensure the complete decomposition of $Li_2C_4O_4$, and then, their electrochemical performance was characterized.

Slightly different cycling protocols and cell configurations were used for the electrodes analyzed by XPS. Since AC-$Li_2C_4O_4$ positive electrodes are considered the cornerstone of the study and the integration of $Li_2C_4O_4$ in those electrodes was optimized, AC-$Li_2C_4O_4$ electrodes were evaluated by using 3-electrode Swagelok cells in a full-cell configuration. The cells were assembled using AC-$Li_2C_4O_4$ positive electrode, HC negative electrode, and Li metal reference electrode, and cycled at $C_{Li2C4O4}$/10 between 2 and 4.2 V (corresponding with a positive electrode swing of ca. 2.5—4.2 V *vs* Li^+/Li). In the case of AC electrodes, they were cycled in a half-cell configuration between 2.5 and 4.2 V versus Li^+/Li to mimic the potential window of the electrodes in a full-cell configuration. AC_{CMC} and AC_{CMC}-$Li_2C_4O_4$ were also characterized in half-cell configuration between 2.5 and 4V versus Li^+/Li prior to the XPS analysis. Half-cell configuration was chosen based on the impossibility of prelithiating the LIC when AC and AC_{CMC} were used, and on the unknown pre-lithiation of HC negative electrodes when $Li_2C_4O_4$ is used in 1 M $LiClO_4$ in EC : DMC electrolyte, which would require the optimization of the system prior to the proper operation of the cells.

Both the applied current density (A g^{-1}) and the calculated specific capacity (mAh g^{-1}) were presented per mass of active mass (AM) in the electrodes unless another metric is indicated. Selected AC-$Li_2C_4O_4$ and AC electrodes had an AM mass loading of ca. 8 mg_{AM} cm^{-2}, while the AC_{CMC}-$Li_2C_4O_4$ electrodes had a mass loading ca. 2 mg_{AM} cm^{-2}. Fluorine-free electrodes pose lower mass loading due to the difficulties found during the water-based processing; nevertheless, since not the electrochemical behavior but the surface chemical composition is studied, a trustful comparison can be established. HC electrodes had a mass loading of ca. 4.5 mg_{AM} and cm^{-2}. Self-standing electrode mass loading was >25 mg_{AM} cm^{-2}. Whatman D-type glass fiber discs of 13 mm in diameter were selected as separators. 1 M $LiPF_6$ in EC : DMC (ethylene carbonate : dimethyl carbonate, 1 : 1 v/v) (99%, Sigma–Aldrich) was used as electrolyte. In the fluorine-free systems, 1 M $LiClO_4$ EC : DMC (1 : 1 v/v) electrolyte was employed.

Conflict of Interest

The authors declare no conflict of interest.

Data Availability Statement

The data that support the findings of this study are available from the corresponding author upon reasonable request.

Keywords: activated carbon · dilithium squarate · interface · lithium-ion capacitor · pre-lithiation

[1] G. G. Amatucci, F. Badway, A. D. Pasquier, T. Zheng, *J. Electrochem. Soc.* **2001**, *148*, A930.
[2] L. Caizán-Juanarena, M. Arnaiz, E. Gucciardi, L. Oca, E. Bekaert, I. Gandiaga, J. Ajuria, *Adv. Energy Mater.* **2021**, *11*, 2100912.
[3] M. Arnaiz, J. Ajuria, *Batteries Supercaps* **2021**, *4*, 733.
[4] M. Arnaiz, D. Shanmukaraj, D. Carriazo, D. Bhattacharjya, A. Villaverde, M. Armand, J. Ajuria, *Energy Environ. Sci.* **2020**, *13*, 2441.
[5] C. Sun, X. Zhang, C. Li, K. Wang, X. Sun, Y. Ma, *Energy Storage Mater.* **2020**, *32*, 497.
[6] J. Jiang, Z. W. Li, Z. T. Zhang, S. J. Wang, H. Xu, X. R. Zheng, Y. X. Chen, Z. C. Ju, H. Dou, X. G. Zhang, *Rare Met.* **2020**, *41*, 3322.
[7] A. Gomez-Martin, M. M. Gnutzmann, E. Adhitama, L. Frankenstein, B. Heidrich, M. Winter, T. Placke, *Adv. Sci.* **2022**, *9*, 2201742.
[8] M. Granados-Moreno, M. Arnaiz, E. Gucciardi, N. E. Asres, E. Goikolea, J. Ajuria, *ChemElectroChem* **2025**, *11*, e202400117.
[9] D. Shanmukaraj, S. Grugeon, S. Laruelle, G. Douglade, J.-M. Tarascon, M. Armand, *Electrochem. Commun.* **2010**, *12*, 1344.
[10] X. Pan, A. Chojnacka, F. Béguin, *Energy Storage Mater.* **2021**, *40*, 22.
[11] L. J. Krause, V. L. Chevrier, L. D. Jensen, T. Brandt, *J. Electrochem. Soc.* **2017**, *164*, A2527.
[12] O. Chusid, E. E. Ely, D. Aurbach, M. Babai, Y. Carmeli, *J. Power Sources* **1993**, *43*, 47.
[13] D. Aurbach, Y. Ein-Eli, O. Chusid, Y. Carmeli, M. Babai, H. Yamin, *J. Electrochem. Soc.* **1994**, *141*, 603.
[14] Y. Ein-Eli, B. Markovsky, D. Aurbach, Y. Carmeli, H. Yamin, S. Luski, *Electrochim. Acta* **1994**, *39*, 2559.
[15] M. Granados-Moreno, R. Cid, M. Arnaiz, E. Goikolea, J. Ajuria, *ACS Appl. Mater. Interfaces* **2024**, *16*, 61846.
[16] S. Fleischmann, J. B. Mitchell, R. Wang, C. Zhan, D. Jiang, V. Presser, V. Augustyn, *Chem. Rev.* **2021**, *120*, 6738.
[17] T. Brousse, M. Toupin, D. Bélanger, *J. Electrochem. Soc.* **2004**, *151*, A614.
[18] C. Yi, J. Zou, H. Yang, X. Leng, *Trans. Nonferrous Met. Soc. China* **2018**, *28*, 1980.
[19] G. Moreno-Fernández, J. L. Gómez-Urbano, M. Enterria, R. Cid, J. M. L. del Amo, R. Mysyk, D. Carriazo, *Electrochim. Acta* **2020**, *361*, 136985.
[20] Q. Abbas, R. Raza, I. Shabbir, A. G. Olabi, *J. Sci.: Adv. Mater. Devices* **2019**, *4*, 341.
[21] C. Huang, A. M. Puziy, O. I. Poddubnaya, D. Hulicova-Jurcakova, M. Sobiesiak, B. Gawdzik, *Electrochim. Acta* **2018**, *270*, 339.
[22] W. Zhu, D. Shen, H. Xie, *Energy Fuels* **2023**, *37*, 12467.
[23] D. D. Zhai, M. Wang, H. Liu, X. Y. Chen, Z. J. Zhang, *Energy Technol.* **2019**, *7*, 1900105.
[24] Y. Fang, B. Luo, Y. Jia, X. Li, B. Wang, Q. Song, F. Kang, L. Zhi, *Adv. Mater.* **2012**, *24*, 6348.
[25] H. Liu, X. Zhang, C. Li, S. Zhao, Y. An, X. Sun, K. Wang, Y. Ma, *ChemSusChem* **2025**, *18*, e202401365.
[26] H. Du, Y. Yang, C. Zhang, Y. Li, J. Wang, K. Zhao, C. Lu, D. Sun, C. Lu, S. Chen, X. Ma, *J. Power Sources* **2024**, *614*, 234988.
[27] G. Lota, E. Frackowiak, *Fuel Cells* **2010**, *10*, 848.
[28] T. Kwon, H. Nishihara, H. Itoi, Q.-H. Yang, T. Kyotani, *Langmuir* **2009**, *25*, 11961.
[29] D. Hulicova-Jurcakova, M. Kodama, S. Shiraishi, H. Hatori, Z. H. Zhu, G. Q. Lu, *Adv. Funct. Mater.* **2009**, *19*, 1800.
[30] W. Yang, W. Yang, A. Song, L. Gao, L. Su, G. Shao, *J. Power Sources* **2017**, *359*, 556.
[31] K. Zou, P. Cai, X. Cao, G. Zou, H. Hou, X. Ji, *Curr. Opin. Electrochem.* **2020**, *21*, 31.
[32] M. Canal-Rodríguez, M. Arnaiz, N. Rey-Raap, A. Arenillas, J. Ajuria, *Electrochim. Acta* **2023**, *463*, 142809.
[33] E. Pameté, L. Köps, F. A. Kreth, S. Pohlmann, A. Varzi, T. Brousse, A. Balducci, V. Presser, *Adv. Energy Mater.* **2023**, *13*, 2301008.
[34] O. E. Eleri, F. Huld, J. Pires, W. M. Tucho, P. Schweigart, A. M. Svensson, F. Lou, Z. Yu, *Electrochim. Acta* **2023**, *453*, 142359.
[35] F. A. Kreth, L. H. Hess, A. Balducci, *Energy Storage Mater.* **2023**, *56*, 192.
[36] S. Malmgren, K. Ciosek, M. Hahlin, T. Gustafsson, M. Gorgoi, H. Rensmo, K. Edström, *Electrochim. Acta* **2013**, *97*, 23.
[37] Q. Xia, H. Yang, M. Wang, M. Yang, Q. Guo, L. Wan, H. Xia, Y. Yu, *Adv. Energy Mater.* **2017**, *7*, 1701336.
[38] Z. Xu, R. Li, G. Xie, D. Qian, H. Fang, Z. Wang, *Energy Storage Mater.* **2024**, *66*, 103195.
[39] S. Ishimoto, Y. Asakawa, M. Shinya, K. Naoi, *J. Electrochem. Soc.* **2009**, *156*, A563.
[40] I. Azcarate, W. Yin, C. Méthivier, F. Ribot, C. Laberty-Robert, A. Grimaud, *J. Electrochem. Soc.* **2020**, *167*, 080530.
[41] C. Peschel, F. Horsthemke, M. Leißing, S. Wiemers-Meyer, J. Henschel, M. Winter, S. Nowak, *Batteries Supercaps* **2020**, *3*, 1183.
[42] F. Holtstiege, P. Bärmann, R. Nölle, M. Winter, T. Placke, *Batteries* **2018**, *4*, 4.
[43] T. Adinaveen, J. J. Vijaya, L. J. Kennedy, *Arab. J. Sci. Eng.* **2016**, *41*, 55.
[44] H. Banda, S. Périé, B. Daffos, P.-L. Taberna, L. Dubois, O. Crosnier, P. Simon, D. Lee, G. De Paëpe, F. Duclairoir, *ACS Nano* **2019**, *13*, 1443.
[45] J. H. Lee, W. H. Shin, M.-H. Ryou, J. K. Jin, J. Kim, J. W. Choi, *ChemSusChem* **2012**, *5*, 2328.
[46] P. Verma, P. Maire, P. Novák, *Electrochim. Acta* **2010**, *55*, 6332.
[47] D. Aurbach, B. Markovsky, I. Weissman, E. Levi, Y. Ein-Eli, *Electrochim. Acta* **1999**, *45*, 67.
[48] M. P. Seah, *Surf. Interface Anal.* **2012**, *44*, 1353.
[49] A. Jablonski, C. J. Powell, *J. Electron Spectrosc. Relat. Phenom.* **2017**, *218*, 1.
[50] M. R. Alexander, G. E. Thompson, X. Zhou, G. Beamson, N. Fairley, *Surf. Interface Anal.* **2002**, *34*, 485.
[51] U. Bhattacharjee, S. Bhowmik, S. Ghosh, S. K. Martha, *Sustainable Energy Fuels* **2023**, *7*, 2321.
[52] J. Maibach, F. Lindgren, H. Eriksson, K. Edström, M. Hahlin, *J. Phys. Chem. Lett.* **2016**, *7*, 1775.
[53] K. C. Högström, S. Malmgren, M. Hahlin, M. Gorgoi, L. Nyholm, H. Rensmo, K. Edström, *Electrochim. Acta* **2014**, *138*, 430.
[54] *Studies in Surface Science and Catalysis*, (Ed: J. Bénard) Adsorption on Metal Surfaces, Vol. *13*, Elsevier, Amsterdam, Oxford, New York **1983**, pp. 150–176.
[55] K. Akada, S. Obata, K. Saiki, *ACS Omega* **2019**, *4*, 16531.
[56] Y. Huang, Y. Zhao, Q. Gong, M. Weng, J. Bai, X. Liu, Y. Jiang, J. Wang, D. Wang, Y. Shao, M. Zhao, *Electrochim. Acta* **2017**, *228*, 214.
[57] N. E. Ghossein, A. Sari, P. Venet, S. Genies, P. Azaïs, *J. Energy Storage* **2021**, *33*, 102039.
[58] P. Azaïs, L. Duclaux, P. Florian, D. Massiot, M.-A. Lillo-Rodenas, A. Linares-Solano, J.-P. Peres, C. Jehoulet, F. Béguin, *J. Power Sources* **2007**, *171*, 1046.
[59] H.-H. Shen, C.-C. Hu, *J. Electrochem. Soc.* **2014**, *161*, A1828.
[60] F. Jeschull, J. Maibach, R. Félix, M. Wohlfahrt-Mehrens, K. Edstrom, M. Memm, D. Brandell, *ACS Appl. Energy Mater.* **2018**, *1*, 5176.
[61] M. Arnaiz, M. Canal-Rodríguez, S. Martin-Fuentes, D. Carriazo, A. Villaverde, J. Ajuria, *J. Phys. Energy* **2023**, *6*, 015001.
[62] D. Bhattacharjya, M. Arnaiz, M. Canal-Rodríguez, S. Martin, T. Panja, D. Carriazo, A. Villaverde, J. Ajuria, *J. Electrochem. Soc.* **2021**, *168*, 110544.
[63] M. Dahbi, F. Ghamouss, F. Tran-Van, D. Lemordant, M. Anouti, *J. Power Sources* **2011**, *196*, 9743.
[64] G. Huang, J. Liang, X. Zhong, H. Liang, C. Cui, C. Zeng, S. Wang, M. Liao, Y. Shen, T. Zhai, Y. Ma, *Nano Res.* **2023**, *16*, 3872.
[65] J. M.ínez De Ilarduya, L. Otaegui, M. Galcerán, L. Acebo, D. Shanmukaraj, T. Rojo, M. Armand, *Electrochim. Acta* **2019**, *321*, 134693.
[66] M. Arnaiz, E. Goikolea, T. Rojo, L. Wittscher, A. Balducci, J. Ajuria, *J. Power Sources* **2019**, *434*, 226757.
[67] K. S. Teoh, M. Melchiorre, S. D. Magar, M. Hermesdorf, D. Leistenschneider, M. Oschatz, F. Ruffo, J. L. Gómez Urbano, A. Balducci, *Adv. Mater.* **2024**, *36*, 2310056.
[68] N. Fairley, V. Fernandez, M. Richard-Plouet, C. Guillot-Deudon, J. Walton, E. Smith, D. Flahaut, M. Greiner, M. Biesinger, S. Tougaard, D. Morgan, *Appl. Surf. Sci. Adv.* **2021**, *5*, 100112.
[69] I. Azpitarte, U. Eletxigerra, A. Barros, E. Aranzabe, R. Cid, *Batteries* **2023**, *9*, 39.

Manuscript received: June 30, 2025
Revised manuscript received: September 3, 2025
Version of record online: